

Multi-frame Feature Aggregation for Real-time Instrument Segmentation in Endoscopic Video

Shan Lin, Fangbo Qin, Haonan Peng, Randall A. Bly, Kris S. Moe, Blake Hannaford*, *Fellow, IEEE*

Abstract—Deep learning-based methods have achieved promising results on surgical instrument segmentation. However, the high computation cost may limit the applications of deep models to time-sensitive tasks such as online surgical video analysis for robotic-assisted surgery. Also, current performance may still suffer from challenging conditions in surgical images such as various lighting conditions and the presence of blood. We propose a novel Multi-frame Feature Aggregation (MFFA) module that leverages information of neighboring frames for segmentation while reducing the influence of spatial misalignment between frames. The MFFA module also further aggregates features spatially based on the spatial self-attention mechanism. Neighboring frames usually have similar appearances, so we consider feature aggregation over a frame sequence as an iterative feature aggregation procedure. By distributing the computational workload of deep feature extraction over each frame in a sequence, we can use a lightweight encoder to reduce the computation costs. Moreover, public surgical videos usually are not labeled by frame, so we develop a method that can randomly synthesize a surgical frame sequence from a labeled frame to assist network training. We demonstrate that our approach achieves superior performance to corresponding deeper segmentation models on a public endoscopic sinus surgery dataset.

I. INTRODUCTION

Surgical videos provide guidance information that surgeons rely on during operations. As video-assisted surgery and robotic-assisted surgery become more integrated, analyzing surgical videos becomes more essential. Surgical video instrument segmentation is one important task that can provide instrument locations to robotic and computer-assisted surgery systems [1], [2], [3].

Challenging conditions in surgical videos such as various lightning scenarios and blood make instrument segmentation a hard problem. For some challenging data, identifying the instrument regions without looking into its adjacent frames can be hard even for human eyes [4]. Surgical videos are readily available, so algorithms that could leverage the temporal information from adjacent video frames for better segmentation on the target frame are attractive. Although Convolutional Neural Networks (CNN) have been successfully applied in surgical instrument segmentation [3], [5], [6], [7], existing works usually perform segmentation on a single frame while the temporal information is not considered.

Recurrent Neural Networks (RNNs) are typical models for temporal sequences and have been successfully applied in

Shan Lin, Haonan Peng, Randall A. Bly, Kris S. Moe and Blake Hannaford are with University of Washington, Seattle, WA 98195, USA.
shan13@uw.edu

Fangbo Qin is with Institute of Automation, Chinese Academy of Sciences, Beijing 100190, China qinfangbo2013@ia.ac.cn

many natural language processing problems [8], [9]. Despite the potential benefits of applying RNNs to image segmentation, RNNs have not been widely studied in instrument segmentation problems for several reasons. The complex gate mechanisms and difficulty of training limit the use of RNNs in image segmentation [10], [11]. Also, RNNs usually require long temporal sequences for training and lead to a high computation burden especially for computer vision problems.

Aggregating features from a few neighboring frames using convolution or spatial-temporal attention-based methods is one alternative strategy to circumvent the problems of RNNs training [12]. In this work, we develop a Multi-frame Feature Aggregation (MFFA) module that consists of a Temporal Aggregation Block (TAB) and a Spatial Aggregation Block (SAB). The TAB is designed to aggregate features of the current frame using the feature maps of the previous frame in a sequence. SAB is then used to further aggregate features for segmentation based on the semantic relationships between different positions in the feature maps. Because the MFFA module keeps passing and aggregating features through each sequence, we propose to use a lightweight encoder feature extractor to reduce the computation cost.

Moreover, public surgical videos usually are not labeled by frame [13], [14]. In many public datasets, frames are extracted from videos with a certain sub-sampling rate for labeling, so a sequence of neighboring frames usually have only one frame labeled. The sparsity of labeling may make the network hard to train in the early iterations. To address this problem, we propose a novel but simple data augmentation method that can synthesize a frame sequence from a single labeled frame. We randomly generate an instrument movement trajectory near the instrument location of a labeled frame, then crop and move the instrument accordingly to generate synthetic frames which form a synthetic sequence. These synthetic sequences are used in the first half of the training procedure.

This paper is among the first few studies that use the information of neighboring video frames for instrument segmentation. We evaluate our method on a public endoscopic sinus surgery dataset. The experiment results demonstrate that by combining the proposed feature aggregation module MFFA with an existing segmentation model, we achieve promising segmentation performance with low computation costs.

II. RELATED WORKS

Surgical Instrument Segmentation Vision-based surgical instrument segmentation aims to divide the surgical images

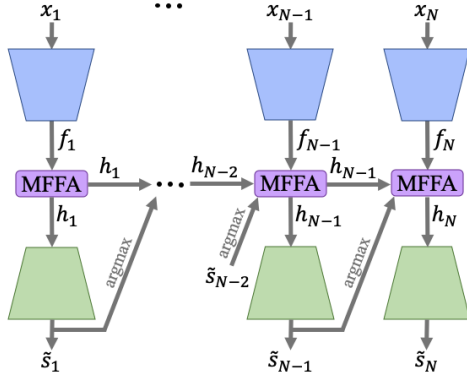


Fig. 1. Schematic of combining the MFFA module with a general encoder-decoder segmentation model. MFFA is inserted between the encoder (represented by a blue trapezoid) and the decoder (represented by a green trapezoid). Note that there is only one encoder-MFFA-decoder architecture, which is repeated for showing how features are passed in a frame sequence.

into instrument and background regions. Deep CNN models have achieved promising segmentation results on single images [15], [16], [5], [17], [18], [19], [3], [7], [6], but the segmentation performance still suffers from challenging conditions in surgical images such as various lightning scenarios, blood and smoke. Recently, feature aggregation based on the relationships between pixels or channels has attracted more attention for robust instrument segmentation. Attia *et. al* developed a RNN that models the spatial dependencies between neighboring pixels to refine segmentation results [20]. Ni *et. al* used relationships between feature channels to emphasize instrument regions for better segmentation [21]. Additionally, Jin *et. al* proposed to propagate segmentation results of the previous frame using motion flow as prior information to assist segmentation and showed that using temporal information could improve the model robustness [22]. Although initial works have shown promising results, studies that leverage temporal and spatial information for instrument segmentation are still limited.

Temporal Information for Video Analysis As typical models for modeling temporal behaviors, RNNs have been widely used in many video analysis tasks such as video captioning, summarization, deblurring, and achieved state-of-the-art performance [23], [24], [25], [26]. In contrast, the applications of RNNs in video semantic segmentation are limited due to difficulties in training RNNs and high computation cost. Feature aggregation over a few neighboring frames has been proposed as an alternative approach to leverage temporal information for segmentation [12]. Another approach is to propagate the segmentation of the previous frame to assist segmentation on the current frame and has achieved promising results with limited annotations [27], [28].

III. METHODS

We develop a Multi-frame Feature Aggregation (MFFA) module that aggregates features for segmentation using both temporal and spatial information. The MFFA module is designed to be flexibly combined with general encoder-decoder segmentation models as introduced in Section III-

A. The architecture of the MFFA module is presented in Section III-B. we also perform an initial investigation on using synthetic sequences with every frame labeled to compensate for lacking densely labeled real frame sequences. The proposed method of generating a labeled synthetic frame sequence from a labeled single frame is described in Section III-C.

A. Task Description and Overall Framework

Given an input sequence with N video frames $X = \{x_1, x_2, \dots, x_N\}$, where x_i is the i th frame in the sequence. The task is to predict the corresponding binary masks $Y = \{\tilde{y}_1, \tilde{y}_2, \dots, \tilde{y}_N\}$, where \tilde{y}_i indicates the predicted instrument and background regions of x_i . For some x_i , the corresponding ground truth label y_i is available for training or testing.

The overall proposed framework is shown in Fig. 1. Instead of segmenting each frame separately, we propose a MFFA module to aggregate features from the previous image in a sequence and pass the aggregated features to the next frame. The MFFA module is designed to combine with general segmentation models that have an encoder-decoder architecture by inserting MFFA between the encoder and the decoder. After obtaining the feature maps f_i outputted from the encoder, f_i , the previous output of MFFA h_{i-1} , and the previous predicted segmentation mask \tilde{y}_{i-1} are inputted into MFFA to generate aggregated feature maps h_i . h_i then serves both as the features passed to the next frame and the input to the decoder for segmenting the current frame. Finally, the encoder generates a softmax output \tilde{s}_i . The segmentation mask \tilde{y}_i is then calculated with argmax from \tilde{s}_i .

Considering that the feature maps are propagated and aggregated through frame sequences that usually consist of frames with similar appearance, the proposed model could be considered as iterative feature aggregation. Therefore, we propose to use lightweight encoders to extract f_i by using the features generated from the middle layers of the deep encoder of the original segmentation model. More specifically, we evaluate the proposed methods on a CNN segmentation model DeepLabV3+ [19] with two different backbone feature extractors, ResNet50 [29] and MobileNet [30]. We use ResNet50 from the beginning to block3 as its lightweight version named ResNet50-b3 [29]. We use MobileNet from the beginning to the 8th pointwise convolution as the lightweight version named MobileNet-p8 [30].

For training, we calculate the naive cross-entropy loss to evaluate segmentation performance for every \tilde{s}_i that has corresponding ground truth y_i . After getting the one-hot encoding for y_i as s_i , the cross-entropy loss can be calculated as

$$\mathcal{L}_{CE}(s_i, \tilde{s}_i) = -\frac{1}{M} \sum_k (s_i)_k \log(\tilde{s}_i)_k \quad (1)$$

where M is the number of elements in the softmax map, $(s_i)_k$ is the k th element of s_i and $(\tilde{s}_i)_k$ is the k th element of \tilde{s}_i . When the network is trained with synthetic frame sequences that have every frame labeled, we pass the sequence both forward and backward and calculate the corresponding

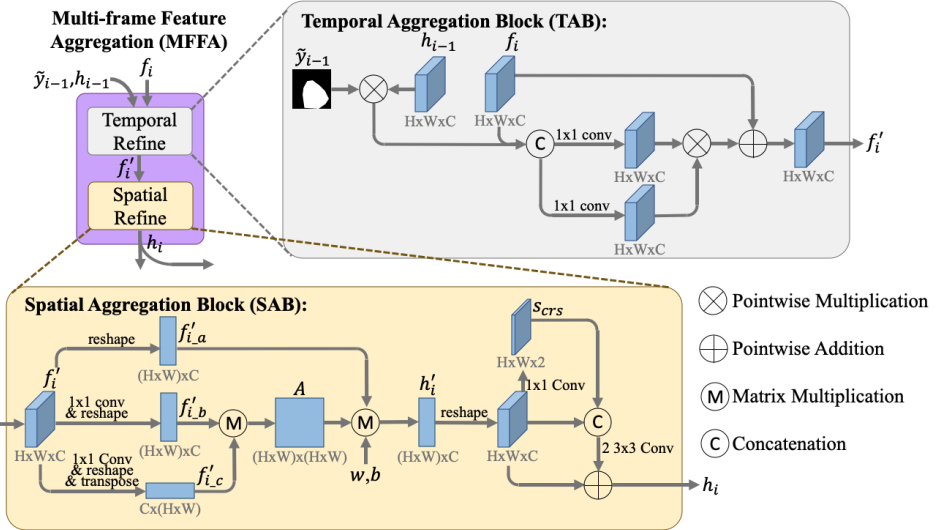


Fig. 2. Schematic of the proposed MFFA module. The MFFA module consists of a Temporal Aggregation Block (TAB) and a Spatial Aggregation Block (SAB).

average cross-entropy loss of all frames. The forward and backward average cross-entropy losses are given by

$$\mathcal{L}_{fw} = \frac{1}{N} \sum_{i=1}^N \mathcal{L}_{CE}(s_i, \tilde{s}_i) \quad (2)$$

$$\mathcal{L}_{bw} = \frac{1}{N} \sum_{i=N}^1 \mathcal{L}_{CE}(s_i, \tilde{s}_i) \quad (3)$$

where N is the number of frames in a sequence. When the network is trained with the real frame sequences that have only the last frame labeled, we pass the sequence forward and evaluate the segmentation accuracy on the last image. We use \mathcal{L}_{last} to represent this loss and it is given by

$$\mathcal{L}_{last} = \mathcal{L}_{CE}(s_N, \tilde{s}_N) \quad (4)$$

For each synthetic or real sequence, there is only one labeled real frame. To guarantee the network could extract good enough features from the first frame in the sequence which does not have features propagated from the previous frame, we input the labeled real frame into the model and calculate its cross-entropy loss \mathcal{L}_{1st} . Assume x_k is the real labeled frame in a sequence, then we have

$$\mathcal{L}_{1st} = \mathcal{L}_{CE}(s_k, \tilde{s}_k) \quad (5)$$

Finally, when the synthetic sequences are used for training, the overall objective function is given by

$$\mathcal{L} = \lambda_1 \mathcal{L}_{fw} + \lambda_2 \mathcal{L}_{bw} + \lambda_3 \mathcal{L}_{1st} \quad (6)$$

When the real sequences are used for training, the overall objective function is given by

$$\mathcal{L} = \lambda_4 \mathcal{L}_{last} + \lambda_5 \mathcal{L}_{1st} \quad (7)$$

where λ_i are hyper-parameters that balance the impact of the losses. In this work, we choose $\lambda_1 = \lambda_2 = \lambda_3 = \frac{1}{3}$ and $\lambda_4 = \lambda_5 = \frac{1}{2}$.

B. Multi-frame Feature Aggregation (MFFA)

The MFFA module consists of a Temporal Aggregation Block (TAB) and a Spatial Aggregation Block (SAB) in series as shown in Fig. 2. MFFA requires \tilde{y}_{i-1} , h_{i-1} and f_i as inputs and outputs h_i . In endoscopic sinus surgery, the instrument regions can be very similar to the background due to strong specular reflection or the presence of blood [14]. Because instrument locations are usually close in neighboring video frames, we propose to emphasize the instrument regions of f_i by only using the instrument features of h_{i-1} for aggregation in TAB. The instrument features are extracted by element-wise multiplication between the previous output \tilde{y}_{i-1} and h_{i-1} . The extracted previous instrument features and current features are then concatenated and passed to two parallel 1×1 convolutions. One of the convolutions performs feature aggregation. The other convolution estimates the similarity between the previous and current feature maps and serves as a gate that assigns higher weights to more similar regions. The outputs of these two convolutions are element-wisely multiplied and then added by f_i to generate f'_i as the output of TAB. When applying MFFA to the first frame in a sequence, previous output and features are not available so we skip TAB and directly input f_i to SAB.

After temporal feature aggregation in TAB, the generated features f'_i is further aggregated using SAB based on spatial relationships. SAB is inspired by the spatial self-attention module [31] and Graph Attention Network (GAT) [32]. Given $f'_i \in \mathbb{R}^{H \times W \times C}$, f'_i can be considered as a graph with $H \times W$ vertices. To estimate the edge values of the graph, we use part of the spatial self-attention module to calculate a spatial attention matrix $A \in \mathbb{R}^{(H \times W) \times (H \times W)}$ [31]. Specifically, f'_i is passed to two parallel 1×1 convolutions for generating two new feature maps $\{f'_{i,b}, f'_{i,c}\} \in \mathbb{R}^{H \times W \times C}$, which are then reshaped to $\mathbb{R}^{(H \times W) \times C}$. Next we transpose $f'_{i,c}$ to $\mathbb{R}^{C \times (H \times W)}$ and perform matrix multiplication between $f'_{i,b}$ and $f'_{i,c}$ to get the spatial attention matrix A . Each element of A represents the similarity between

the corresponding positions in f'_i . Then we reshape f'_i to $\mathbb{R}^{(H \times W) \times C}$ and aggregate the vertices features using A through matrix multiplication. After that we use trainable parameters $w \in \mathbb{R}^{C \times C}$ and bias $b \in \mathbb{R}^C$ to get a refined features h'_i as inspired by [32]. The expression of this process is given by

$$h'_i = Af'_{i,a}w + b \quad (8)$$

After reshaping h'_i from $\mathbb{R}^{(H \times W) \times C}$ to $\mathbb{R}^{H \times W \times C}$, we further refine the features using a ResNet module-like block as proposed in [33]. Specifically, h'_i goes through a 1×1 convolution and the softmax function to generate a coarse segmentation results \tilde{s}_{crs} . Finally, the output of SAB is obtained by

$$h_i = h'_i + \Phi(h'_i, \tilde{s}_{crs}) \quad (9)$$

where $\Phi(a, b)$ performs a and b concatenation followed by two 3×3 convolution filters in series [33].

C. Synthetic Frame Sequence

We propose a method that can generate a frame sequence with every frame labeled from one real labeled frame. The proposed frame sequence synthetic method is developed based on the data augmentation method introduced in [34]. In [34], the training set for instance segmentation was augmented by cropping and randomly jittering the target objects in images. The hole left by the moved target objects were then filled with an off-the-shelf inpainting method [35]. Refer to [34] for more implementation details.

Different from [34], we need frame sequences with each frame labeled for training. Given a real frame x and its label y , our goal is to generate a synthetic frame sequence with N labeled frames $S = \{s_1, s_2, \dots, s_N\}$. We first put x to the center of the target sequence, i.e. let $s_C = x$ where $C = \lfloor \frac{N+1}{2} \rfloor$. For the instrument in the i th frame, we define its translations on the x and y-axis and the rotation with respect to the instrument in x as dx_i, dy_i and $d\theta_i$, which are called moving parameters. Then we randomly select the moving parameters for the first and the last frames (i.e., $dx_0, dy_0, d\theta_0, dx_N, dy_N, d\theta_N$) and use linear interpolation to decide the moving parameters of the other frames in the target sequence. Finally, the instruments are cropped, rotated and moved to corresponding locations using the aforementioned augmentation method to generate all synthetic frames that form the target sequence. We also apply the same process with the same moving parameters on y to get the corresponding labels. Figure 3 shows examples of synthetic frame sequences.

IV. DATASETS

We evaluate our model on a public endoscopic sinus surgery dataset UW-Sinus-Surgery-C/L, which consists of a cadaver and a live dataset [14]. The cadaver dataset consists of 10 5-minute to 23-minute cadaveric surgery videos with a resolution of 320×240 . A total of 4345 frames were extracted with a sampling rate of 0.5 Hz from the videos. The instrument regions were labeled for semantic segmentation. The live dataset consists of 3 12-minute to 66-minute live

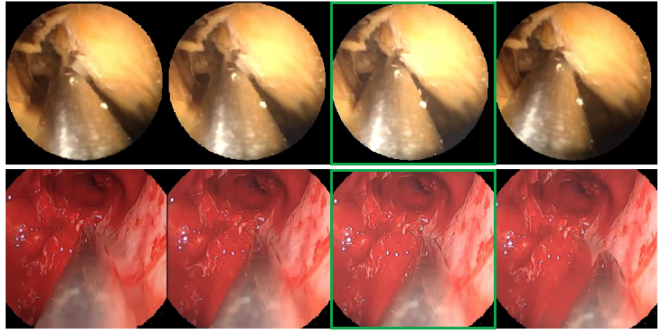


Fig. 3. Examples of synthetic frame sequences. The top row is a sequence generated from a cadaveric surgical frame and the bottom row is a sequence generated from a live surgical frame. The real frames are bounded by green boxes and others are synthetic frames augmented from the real frames. Refer to Section IV for more information of the datasets.

surgery videos with a resolution of 1920×1080 . Similarly, a total of 4658 frames were extracted with a sampling rate of 1 Hz and labeled.

The main difficulties of this dataset include specular reflections, blur from motion, blood and smoke. In both cadaveric and live surgery videos, strong specular reflections make the instruments have similar appearances to the background. In the live surgery videos, segmentation becomes even harder with instruments attached by blood. The instruments are usually used under lower speeds during surgery, but senior surgeons who are more familiar with the anatomies may move instruments faster especially when they switch the surgery sites. Moreover, the smoke generated when electrocauteries are used can make the instruments hard to identify. Considering that these challenging conditions usually are not consistent through the entire video but switch between each other, so temporal information from neighboring frames could be useful to improve segmentation performance.

Endoscopic frames have large black border regions that contain no useful information, so we extracted frame center regions and downsampled them to 240×240 for segmentation. To evaluate the generalization ability of our model, we performed K-fold cross-validation with $K = 3$. We use the same fold split rules as stated in [14]. Each fold of the cadaver dataset consists of frames from 3 to 4 videos, and each fold of the live dataset consists of frames from one of the three videos.

V. IMPLEMENTATION DETAILS

The segmentation models were implemented on a 4.20GHz Intel i7-7700K CPU and a Nvidia Titan Xp GPU.

Instrument segmentation models The instrument segmentation models were implemented with or without the proposed MFFA module. The backbone networks of all models were pre-trained on ImageNet. We used Adam optimizer to train each model with 40 epochs and 16 batch size. The learning rate was initialized as 0.0005 and exponentially decayed every 5 epochs from the 20th epoch.

When trained the models without MFFA, we perform data augmentation including i) change the image hue, brightness, saturation and contrast; ii) image flipping, rotation, scaling

TABLE I
SEGMENTATION PERFORMANCE ON UW-SINUS-SURGERY-C/L

Group	Model(Backbone)	Proposed		Performance (mDSC(%) / mIoU(%))		Time (ms)
		MFFA	Synth.	Sinus-Surgery-C	Sinus-Surgery-L	
1	TernausNet-16 [18] (VGG16)	n/a	n/a	85.5(3.6)/80.4(4.3)	80.4(5.7)/74.1(6.60)	13.2
	LWANet [21] (MobileNet)			81.1(3.8)/74.9(4.5)	72.6(7.7)/65.2(8.8)	9.4
	MAFA-DL3+ [36] (ResNet50)			91.2(1.0)/86.8(1.2)	87.7(3.8)/82.1(4.6)	19.8
2	DL3+ [19] (MobileNet)	✗	✗	82.5(2.9)/76.7(3.4)	75.1(7.0)/67.8(8.3)	3.5
	DL3+ [19] (MobileNet-p8)	✓	✗	78.7(3.0)/72.2(3.7)	75.9(7.5)/68.2(8.9)	2.6
	DL3+ [19] (ResNet50)	✓	✓	83.8(2.2)/78.4(2.8)	80.2(5.2)/73.3(6.3)	2.9
	DL3+ [19] (ResNet50-b3)	✗	✗	85.1(1.7)/79.7(2.4)	83.5(3.8)/77.0(4.7)	2.9
3	DL3+ [19] (ResNet50)	✗	✗	86.7(2.4)/81.6(2.9)	80.8(5.0)/74.0(6.2)	8.9
	DL3+ [19] (ResNet50-b3)	✓	✗	84.9(3.7)/79.6(4.3)	80.7(5.4)/73.9(6.6)	5.6
	DL3+ [19] (ResNet50-b3)	✓	✓	86.8(1.9)/81.8(2.5)	84.4(4.4)/78.2(5.3)	5.9
	DL3+ [19] (ResNet50-b3)	✓	✓	88.5(2.2)/83.6(2.7)	85.4(3.3)/79.4(4.1)	6.0

* i) The mDice and mIoU are shown in the form of mean(standard deviation); ii) MobileNet-p8 is the lightweight version of MobileNet; iii) ResNet50-b3 is the lightweight version of ResNet50; iv) Both synthetic and real data are used for training if 'Synth.' is checked, otherwise only real data are used for training; v) The bold font indicates the best performance in the column of each group.

and cropping. We cropped the frames to a resolution of 192×192 to accelerate training, while the full images with a resolution of 240×240 were used for testing. When trained the models with MFFA, we implemented similar data augmentation on the frame sequences. We jittered the appearance of every frame in the sequences independently, while all frames in the same sequence shared the same parameters for flipping, rotation, scaling and cropping.

Synthetic and real frame sequence Each synthetic or real frame sequence consists of 4 frames. To generate synthetic sequences, we need to decide the translations and rotation angles of the instruments in the first and the last frames with respect to the instrument in the labeled frame. The translation values were randomly selected from a uniform distribution over 15 to 40 pixels on both positive/negative x-axis and positive/negative y-axis directions. The rotation angles were randomly selected from a uniform distribution over -30 to 30 degrees. Moreover, real frame sequences were extracted around labeled frames in the videos and each frame in a sequence was sampled out of 3 consecutive frames.

We studied two situations when training models with MFFA: i) Use only the real frame sequences; ii) Use the synthetic frame sequences to train the network in the first 20 epochs and use the real frame sequences to train the network in the left 20 epochs. The second situation is represented with 'Synth.' in Table I and Table III.

VI. EXPERIMENTS AND RESULTS

We combined the proposed MFFA module with DeepLabV3+ (DL3+) [19] (abbreviated as MFFA-DL3+) and compared with the original version of DeepLabV3+ [19] as baseline. MFFA-DL3+ were also compared with advanced segmentation models include TernausNet [18], LWANet [21] and MAFA [36]. For evaluating the segmentation performance, we used Dice similarity coefficient (DSC) and Intersection over Union (IoU) [37], which are defined as

$$DSC = \frac{2|X \cap Y|}{|X| + |Y|}, IoU = \frac{|X \cap Y|}{|X \cup Y|}$$

where X and Y are the predicted and ground truth segmentation masks, respectively.

TABLE II
PAIRED T-TEST RESULTS OF BASELINES (DEEPLABV3+ [19]) AND PROPOSED MODELS

Compared Model (Backbone, Real/Synthetic Data)	p-value
DL3+(MobileNet, R)	DL3+(MobileNet-p8, R)
	MFFA-DL3+(MobileNet-p8, S)
	MFFA-DL3+(ResNet50-b3, S)
DL3+(ResNet50, R)	DL3+(ResNet50-b3, R)
	MFFA-DL3+(MobileNet-p8, S)
	MFFA-DL3+(ResNet50-b3, S)
MFFA-DL3+(MobileNet-p8, R)	MFFA-DL3+(MobileNet-p8, S)
	0.023
MFFA-DL3+(ResNet50-b3, R)	MFFA-DL3+(ResNet50-b3, S)
	0.018

* i) MobileNet-p8 is the lightweight version of MobileNet; ii) ResNet50-b3 is the lightweight version of ResNet50; iii) In the brackets, 'R' represents only real data are used for training, while 'S' represents both synthetic and real data are used for training; iv) The bold font indicates the p-value is less than or equal to the significance level 0.05.

Table I shows the segmentation results on UW-Sinus-Surgery C/L in three groups: i) Group 1 consists of the performance of three advanced segmentation models on single frames; ii) Group 2 consists of the performance of the original version of DL3+(MobileNet) and MFFA-DL3+(MobileNet-p8) with/without using synthetic frame sequences for training; iii) Group 3 consists of the performance of the original version of DL3+(ResNet50) and MFFA-DL3+(ResNet-b3) with/without using synthetic frame sequences for training. Because some data folds have high bias, the mean and standard deviation of mDice and mIoU are not enough for comparing the performance. Therefore, we performed paired t-test on the 6 data folds of UW-Sinus-Surgery C/L together to determine if there are significant differences between the models and the results are shown in Table II. When both synthetic and real frame sequences are used for training, MFFA-DL3+ with reduced backbone achieved superior performance of 1.8%~8.4% better mDice and 2%~9.2% better mIoU with less inference time compared with the baseline DL3+ [19]. Also, MFFA-DL3+(MobileNet-p8) achieved comparable results to DL3+(ResNet50) with only about 33% of the average inference time. Moreover, compared with the three advanced segmentation models shown in group 1, both MFFA-DL3+(MobileNet-p8) and

TABLE III
ABLATION STUDIES OF MFFA WITH DEEPLABV3+ ON UW-SINUS-SURGERY-C/L DATASET

No.	Method					Performance (mDSC(%) / mIoU(%))	
	Backbone	TAB	SAB	Synth.	\mathcal{L}_{1st}	Sinus-Surgery-C	Sinus-Surgery-L
1	MobileNet	✗	✗	✗	✗	82.5(2.9)/76.7(3.4)	75.1(7.0)/67.8(8.3)
2	—	✗	✗	✗	✗	78.7(3.0)/72.2(3.7)	75.9(7.5)/68.2(8.9)
3	—	✗	✓	✗	✗	81.2(2.2)/74.8(2.9)	74.7(8.2)/67.0(9.4)
4	MobileNet-p8	✓	✓	✓	✗	83.9(2.8)/78.1(3.4)	79.2(6.0)/72.3(7.2)
5	—	✓	✓	✓	✓	83.8(2.2)/78.4(2.8)	80.2(5.2)/73.3(6.3)
6	—	✓	✓	✓	✗	84.7(3.2)/79.2(4.0)	80.8(6.3)/74.1(7.5)
7	—	✓	✓	✓	✓	85.1(1.7)/79.7(2.4)	83.5(3.8)/77.0(4.7)

* i) MobileNet-p8 is the lightweight version of MobileNet; ii) Both synthetic and real data are used for training if 'Synth.' is checked, otherwise only real data are used for training; iii) The bold font indicates the best performance in the column.

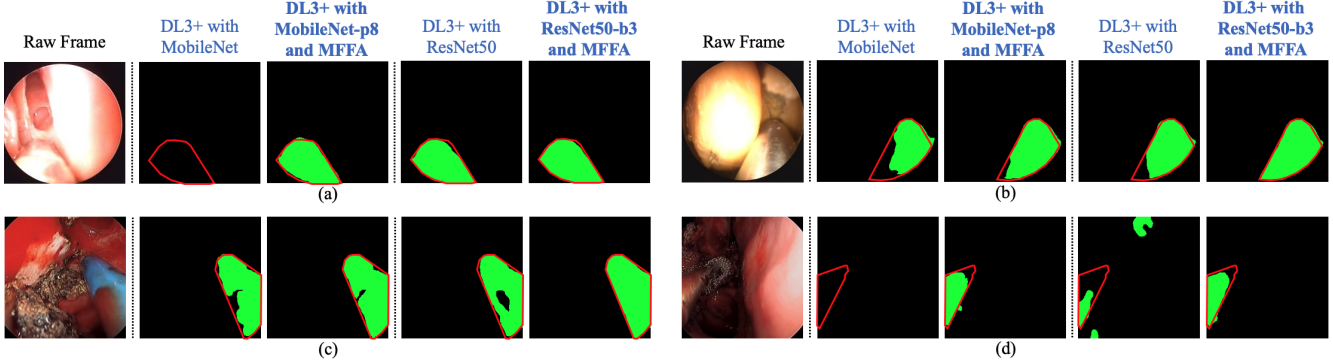


Fig. 4. Examples of segmentation results. In each subfigure, the first frame is the input raw frame and the next four frames are the segmentation results of DeepLabV3+ (DL3+) [19] with MobileNet as the backbone feature extractor, DL3+ with MobileNet-p8 and MFFA, DL3+ with ResNet50, and DL3+ with ResNet50-b3 and MFFA, respectively. MFFA-DL3+(MobileNet-p8) and MFFA-DL3+(ResNet50-b3) were trained with both synthetic and real frame sequences. The predicted instrument regions are drawn in green and the true instrument contours are labeled by red lines. The example results of UW-Sinus-Surgery-C, UW-Sinus-Surgery-L are shown in (a,b) and (c,d), respectively.

MFFA-DL3+(ResNet-b3) achieved superior or comparable performance with much lower computation costs.

To evaluate the effectiveness of each proposed modules i) Temporal Aggregation Block (TAB), ii) Spatial Aggregation Block (SAB) and iii) \mathcal{L}_{1st} , we conducted ablation studies under different configurations. Table III shows the evaluation results with DeepLabV3+ [19]. The original version of DL3+(MobileNet) was used in experiment 1, while DL3+ with a reduced backbone MobileNet-p8 was used in experiment 2~7. Experiment 3 shows that using SAB without temporal feature aggregation improved the performance on the cadaver dataset but didn't influence the performance on the live dataset much. By comparing experiments 4 and 5, and comparing experiments 6 and 7, we found that \mathcal{L}_{1st} is more effective for training that uses synthetic frame sequences.

VII. DISCUSSION

We propose MFFA that performs feature aggregation both temporally and spatially. MFFA could easily be combined with general segmentation models that have an encoder-decoder architecture. By distributing the feature extraction burden to each frame in the sequences, our method can use lightweight encoders and achieve accurate segmentation results with lower computation costs.

Fig. 4 shows some examples of the segmentation results. We found that the proposed MFFA module could help improve instrument segmentation by finding the missing parts in the baseline experiments under many challenging

conditions. In this work, we focus on semantic segmentation in which pixels are classified into different classes without separating different objects. When analyzing surgical videos that have several instruments operate at the same time, instance segmentation that treats objects of the same class separately is more appealing because it provides more information regarding surgical workflow. We will explore leveraging temporal information for instance segmentation as future work.

Although Table II shows that by using the synthetic frame sequences we improved the segmentation performance than using only the real frame sequences, but we think there is still some space left for improvement because the current synthesis method is relatively simple. We choose to simply generate instrument trajectory due to two reasons: i) the frame sequences used in this work have only 4 frames with small instrument movements, so this method provides acceptable approximations to the real sequences. ii) The statistical or other knowledge of instrument moving behaviors are not available in the datasets studied in this work. The true instrument movement pattern could be considered in the future to generate more realistic sequences. One potential option is performing interpolation between two neighboring labeled frames to generate better synthetic trajectories.

VIII. CONCLUSIONS

In this work, we develop a MFFA module that performs feature aggregation based on temporal and spatial relationships between frame pixels to improve instrument

segmentation. By using the MFFA module, we can reduce the deep encoder to its lightweight version and decrease the computation costs. Another advantage of the proposed MFFA module is that it could be easily combined with any segmentation model that has an encoder-decoder architecture. Also, we propose a simple but effective strategy that can generate a synthetic frame sequence from a single labeled frame to assist network training and compensate for a lack of labeled real frame sequences. In the future, we will further improve the frame sequence synthesize approach and apply the proposed method to instance segmentation on surgical videos.

REFERENCES

- [1] D. Bouget, M. Allan, D. Stoyanov, *et al.*, “Vision-based and markerless surgical tool detection and tracking: a review of the literature,” *Medical Image Analysis*, vol. 35, pp. 633–654, 2017.
- [2] M. Allan, S. Kondo, S. Bodenstedt, *et al.*, “2018 robotic scene segmentation challenge,” *arXiv preprint arXiv:2001.11190*, 2020.
- [3] A. A. Shvets, A. Rakhlis, A. A. Kalinin, *et al.*, “Automatic instrument segmentation in robot-assisted surgery using deep learning,” in *Proc. IEEE Int. Conf. Mach. Learn. Appl.*, pp. 624–628, 2018.
- [4] S. Lin, F. Qin, Y. Li, *et al.*, “LC-GAN: Image-to-image translation based on generative adversarial network for endoscopic images,” in *Proc. IEEE Int. Conf. Intell. Robot. Syst.*, 2020.
- [5] L. C. García-Peraza-Herrera, W. Li, L. Fidon, *et al.*, “Toolnet: holistically-nested real-time segmentation of robotic surgical tools,” in *Proc. IEEE Int. Conf. Intell. Robot. Syst.*, pp. 5717–5722, 2017.
- [6] M. Allan, A. Shvets, T. Kurmann, *et al.*, “2017 robotic instrument segmentation challenge,” *arXiv preprint arXiv:1902.06426*, 2019.
- [7] M. Islam, Y. Li, and H. Ren, “Learning where to look while tracking instruments in robot-assisted surgery,” in *Proc. Int. Conf. Med. Image Comput. Comput. Assist. Interv.*, pp. 412–420, 2019.
- [8] Q. Chen, X. Zhu, Z.-H. Ling, *et al.*, “Enhanced LSTM for natural language inference,” in *Proc. Annu. Meeting Assoc. Comput. Linguistics*, pp. 1657–1668, 2017.
- [9] G. Liu and J. Guo, “Bidirectional LSTM with attention mechanism and convolutional layer for text classification,” *Neurocomputing*, vol. 337, pp. 325–338, 2019.
- [10] Z. C. Lipton, J. Berkowitz, and C. Elkan, “A critical review of recurrent neural networks for sequence learning,” *arXiv preprint arXiv:1506.00019*, 2015.
- [11] B. Yu, H. Yin, and Z. Zhu, “Spatio-temporal graph convolutional networks: a deep learning framework for traffic forecasting,” in *Proc. Int. Joint Conf. Artif. Intell.*, pp. 3634–3640, 2018.
- [12] P. Hu, F. Caba, O. Wang, *et al.*, “Temporally distributed networks for fast video semantic segmentation,” in *Proc. IEEE Conf. Comput. Vis. Pattern Recognit.*, pp. 8818–8827, 2020.
- [13] T. Ross, A. Reinke, P. M. Full, *et al.*, “Robust medical instrument segmentation challenge 2019,” *arXiv preprint arXiv:2003.10299*, 2020.
- [14] S. Lin, F. Qin, R. A. Bly, *et al.*, “UW sinus surgery cadaver/live dataset (UW-Sinus-Surgery-C/L),” 2020.
- [15] J. Long, E. Shelhamer, and T. Darrell, “Fully convolutional networks for semantic segmentation,” in *Proc. IEEE Conf. Comput. Vis. Pattern Recognit.*, pp. 3431–3440, 2015.
- [16] O. Ronneberger, P. Fischer, and T. Brox, “U-Net: Convolutional networks for biomedical image segmentation,” in *Proc. Int. Conf. Med. Image Comput. Comput. Assist. Interv.*, pp. 234–241, 2015.
- [17] A. Chaurasia and E. Culurciello, “LinkNet: Exploiting encoder representations for efficient semantic segmentation,” in *Proc. IEEE Visual Commun. Image Process.*, pp. 1–4, 2017.
- [18] V. Iglovikov and A. Shvets, “TernausNet: U-Net with VGG11 encoder pre-trained on imagenet for image segmentation,” *arXiv preprint arXiv:1801.05746*, 2018.
- [19] L. C. Chen, Y. Zhu, G. Papandreou, *et al.*, “Encoder-decoder with atrous separable convolution for semantic image segmentation,” in *Proc. Europ. Conf. Comput. Vis.*, pp. 801–818, 2018.
- [20] M. Attia, M. Hossny, S. Nahavandi, *et al.*, “Surgical tool segmentation using a hybrid deep CNN-RNN auto encoder-decoder,” in *IEEE Int. Conf. Syst., Man, Cybern.*, pp. 3373–3378, 2017.
- [21] Z. L. Ni, G. B. Bian, Z. G. Hou, *et al.*, “Attention-guided lightweight network for real-time segmentation of robotic surgical instruments,” in *Proc. Int. Conf. Robot. Autom.*, pp. 9939–9945, 2020.
- [22] Y. Jin, K. Cheng, Q. Dou, *et al.*, “Incorporating temporal prior from motion flow for instrument segmentation in minimally invasive surgery video,” in *Proc. Int. Conf. Med. Image Comput. Comput. Assist. Interv.*, pp. 440–448, 2019.
- [23] B. Zhao, X. Li, and X. Lu, “CAM-RNN: Co-attention model based rnn for video captioning,” *IEEE Trans. Image Process.*, vol. 28, no. 11, pp. 5552–5565, 2019.
- [24] B. Zhao, X. Li, and X. Lu, “HSA-RNN: Hierarchical structure-adaptive RNN for video summarization,” in *Proc. IEEE Conf. Comput. Vis. Pattern Recognit.*, pp. 7405–7414, 2018.
- [25] T. Hyun Kim, K. Mu Lee, B. Scholkopf, *et al.*, “Online video deblurring via dynamic temporal blending network,” in *Proc. IEEE Int. Conf. Comput. Vis.*, pp. 4038–4047, 2017.
- [26] S. Nah, S. Son, and K. M. Lee, “Recurrent neural networks with intra-frame iterations for video deblurring,” in *Proc. IEEE Conf. Comput. Vis. Pattern Recognit.*, pp. 8102–8111, 2019.
- [27] P. Voigtlaender, Y. Chai, F. Schroff, *et al.*, “Feelvos: Fast end-to-end embedding learning for video object segmentation,” in *Proc. IEEE Conf. Comput. Vis. Pattern Recognit.*, pp. 9481–9490, 2019.
- [28] J. Miao, Y. Wei, and Y. Yang, “Memory aggregation networks for efficient interactive video object segmentation,” in *Proc. IEEE Conf. Comput. Vis. Pattern Recognit.*, pp. 10 366–10 375, 2020.
- [29] K. He, X. Zhang, S. Ren, *et al.*, “Deep residual learning for image recognition,” in *Proc. IEEE Conf. Comput. Vis. Pattern Recognit.*, pp. 770–778, 2016.
- [30] A. G. Howard, M. Zhu, B. Chen, *et al.*, “Mobilenets: Efficient convolutional neural networks for mobile vision applications,” *arXiv preprint arXiv:1704.04861*, 2017.
- [31] J. Fu, J. Liu, H. Tian, *et al.*, “Dual attention network for scene segmentation,” in *Proc. IEEE Conf. Comput. Vis. Pattern Recognit.*, pp. 3146–3154, 2019.
- [32] Y. Lu, Y. Chen, D. Zhao, *et al.*, “CNN-G: Convolutional neural network combined with graph for image segmentation with theoretical analysis,” *IEEE Trans. Cogn. Devel. Syst.*, 2020.
- [33] C. Zhang, G. Lin, F. Liu, *et al.*, “CANet: Class-agnostic segmentation networks with iterative refinement and attentive few-shot learning,” in *Proc. IEEE Conf. Comput. Vis. Pattern Recognit.*, pp. 5217–5226, 2019.
- [34] H. S. Fang, J. Sun, R. Wang, *et al.*, “InstaBoost: Boosting instance segmentation via probability map guided copy-pasting,” in *Proc. IEEE Int. Conf. Comput. Vis.*, pp. 682–691, 2019.
- [35] A. Telea, “An image inpainting technique based on the fast marching method,” *Journal of graphics tools*, vol. 9, no. 1, pp. 23–34, 2004.
- [36] F. Qin, S. Lin, Y. Li, *et al.*, “Towards better surgical instrument segmentation in endoscopic vision: multi-angle feature aggregation and contour supervision,” *IEEE Robot. Autom. Lett.*, 2020.
- [37] A. A. Taha and A. Hanbury, “Metrics for evaluating 3D medical image segmentation: analysis, selection, and tool,” *BMC Medical Imaging*, vol. 15, no. 1, p. 29, 2015.